ENVIRONMENTAL RESEARCH
LETTERS

LETTER

Progress report on addressing meteotsunami risk in the eastern Yellow Sea

Myung-Seok Kim[1], Seung-Buhm Woo[1,*], Hyunmin Eom[2] and Sung Hyup You[2]

[1] Department of Ocean Sciences, Inha University, Incheon 22212, Republic of Korea
[2] Marine Meteorology Division, Korea Meteorological Administration, Seoul 07062, Republic of Korea
* Author to whom any correspondence should be addressed.

E-mail: sbwoo@inha.ac.kr

Keywords: meteotsunami, air pressure oscillation, air pressure jump, monitoring system, lead time, open-ocean buoy

OPEN ACCESS

RECEIVED
27 August 2021

REVISED
24 November 2021

ACCEPTED FOR PUBLICATION
29 November 2021

PUBLISHED
23 December 2021

Original content from this work may be used under the terms of the Creative Commons Attribution 4.0 licence.

Any further distribution of this work must maintain attribution to the author(s) and the title of the work, journal citation and DOI.

Abstract

On 31 March 2007, strong, tsunami-like waves of 1.0–2.5 m were recorded at most tide gauges along the west coast of Korea. The following year, on May 4, unexpected, abnormal waves in the eastern Yellow Sea reached a maximum height of ∼1.3 m. Both events occurred without warning, resulting in severe loss of life and property. Subsequent analysis found that these tsunami-like waves were meteotsunamis generated by air pressure oscillations. Evidence of possible meteotsunamis has been recorded by existing observation systems. However, the lack of understanding of the phenomenon and meteotsunami-specific monitoring system has hindered community preparedness, resulting in severe damage. We utilized existing observation systems (meteorological stations, tide gauges, and radar) during 2018 to develop a real-time meteotsunami monitoring system in the eastern Yellow Sea. This system detects the intensity and propagation of air pressure oscillations to identify potential coastal hazards and prevent damage caused by meteotsunamis. Two air pressure disturbance methods for measuring intensity of air pressure oscillation (a range of pressure changes over a 60 min window vs the rate of pressure change over a 10 min window) were compared, and several test operations were performed during development of the proposed system. The progress and limitations of the current observation and monitoring system were confirmed based on recent monitoring reports of air pressure jumps during the meteotsunamis on 7 April 2019. To address the insufficient lead time of meteotsunami warnings, installation and testing of open-ocean buoys outfitted with pressure sensors commenced in 2019.

1. Introduction

Meteotsunamis, hazardous waves induced by atmospheric processes rather than seismic events, have become well known in contemporary tsunami science (Rabinovich 2020, Vilibić *et al* 2021). Meteotsunamis are generated by various atmospheric disturbances, such as atmospheric gravity waves, frontal passages, squalls, and hurricanes (Rabinovich 2009). Such atmospheric disturbances are related to the propagation of air pressure disturbances, which can trigger meteotsunamis (Šepić *et al* 2012). Destructive meteotsunami events are the consequence of a combination of resonance mechanisms, namely the Proudman, Greenspan, and harbor resonances (Proudman 1929, Greenspan 1956, Monserrat *et al* 2006). Globally, meteotsunamis occur more frequently than seismic tsunamis, but are much less powerful (Pattiaratchi and Wijeratne 2015).

Establishing monitoring and early warning systems for meteotsunamis is challenging as they are generally not observed as strongly as seismic tsunamis in time series. Similar to tsunamis, meteotsunamis—atmospherically induced long ocean waves in a tsunami frequency band—can be observed and identified early based on synoptic forecasting, atmosphere-ocean coupled modeling, and various related observations (Vilibić *et al* 2016). Attempts have been made to develop a simple and low-cost meteotsunami monitoring system by comprehensively utilizing existing systems in each region. In general, the monitoring system's meteotsunami detection protocol is characterized by tracking air pressure disturbances (temporal pressure changes) detected by

© 2021 The Author(s). Published by IOP Publishing Ltd

multiple meteorological stations (Vilibić *et al* 2008, Šepić *et al* 2009). Šepić and Vilibić (2011) suggest it is possible to monitor the occurrence of meteotsunamis at tide gauges with a strong history of recording favorable air pressure disturbance conditions (intensity, speed, and direction) for destructive meteotsunami generation. Recently, radar reflectivity together with land-based pressure data has been utilized to track the propagation of air pressure disturbances (Wertman *et al* 2014, Linares *et al* 2016, Titov and Moore 2021).

Destructive meteotsunami events occurred in the eastern Yellow Sea on 31 March 2007, and again on 4 May 2008, resulting in a great loss of life and property. On 31 March 2007, tsunami-like sea-level oscillations were recorded at most tide gauges in the eastern Yellow Sea, causing ship damage and coastal flooding without warning. Also, as strong atmospheric disturbances were observed at most meteorological stations at the time, many studies on the generation of the hazardous meteotsunamis of 31 March 2007 have been performed (Choi *et al* 2008, Eom *et al* 2012, Kim *et al* 2017). At noon on 4 May 2008, abnormally large waves in front of a breakwater swept away several people. Tragically, 24 people were killed or injured by these waves. The accident scene and killer waves were captured on closed-circuit television (CCTV), but the atmospheric disturbances and sea-level oscillations analyzed from meteorological stations and tide gauges were not as dynamic as those from the event on 31 March 2007. A few years later, the abnormal waves were found to be local air pressure disturbance induced meteotsunamis (Choi and Lee 2009, Ha *et al* 2014). However, the generation mechanism of the significant wave amplification (∼1.3 m) captured by CCTV cameras near the coast is still unknown (Yoo *et al* 2010). Although atmospheric disturbance observations were captured for both events, the occurrence of unexpected meteotsunamis in the absence of a monitoring system resulted in significant loss. There was no meteotsunami monitoring system in the eastern Yellow Sea until 2017. The Korea Meteorological Administration (KMA) has developed a monitoring system, conducted pilot tests, and overseen the expansion of observation systems since 2018.

In this study, we introduce an observational and real-time monitoring system for meteotsunami disaster prevention in the eastern Yellow Sea. This monitoring approach tracks the intensity and propagation of air pressure disturbances that are favorable to meteotsunami occurrence (Kim *et al* 2021a). For better meteotsunami detection, two methods of detecting air pressure disturbance were compared during the development and testing of the proposed monitoring system. After the monitoring system was developed in 2018, the monitoring potential for meteotsunamis was presented in KMA monitoring reports on the air pressure disturbance-induced meteotsunami event of 7 April 2019. We also discuss limitations of the present meteotsunami monitoring system and suggest future improvements.

2. Tsunami-like waves of atmospheric origins

Meteotsunamis approaching from various directions can be identified by the propagation pattern of air pressure disturbances obtained from meteorological and ocean data, such as that provided by the KMA and the Korea Hydrographic and Oceanographic Agency. As of 2021, 494 automatic weather stations (AWSs) were operating in Korea, including in inland areas. Eighty-nine AWSs located along the west coast of Korea are utilized for early warning (figure 1(b)). These AWSs are divided into two zones based on the distance from the coast: 17 AWSs in the caution zone and 72 AWSs in the warning zone. We used mean sea level pressure data obtained at 1 min sampling intervals from the 89 AWSs. The tide gauges along the coastline of Korea are mostly located in harbors and along breakwaters. The swell-induced oscillations were removed during the sampling process at each tide gauge, and sea-level data at 1 min intervals were used. Additionally, radar images were referenced when tracking spatiotemporal variations of atmospheric disturbances in the real-time monitoring system. This is because the reflectivity of the radar image is correlated with atmospheric disturbances (Wertman *et al* 2014, Linares *et al* 2016). There is a plan to install ocean buoys outfitted with pressure sensors in the open sea to improve early detection, as shown by the red dashed box in figure 1(a).

To develop a meteotsunami monitoring system in the eastern Yellow Sea, we identified the characteristics of the meteotsunami event of 31 March 2007; Korea's strongest meteotsunami event at the largest spatial scale to date. From midnight to early morning on 31 March 2007, pressure-forced meteotsunamis occurred as a result of atmospheric disturbances, as shown in figure 2(e), and propagated in succession to the eastern Yellow Sea. As strong air pressure oscillations measured at the KyukRyul (KR) AWS in the caution zone traveled to the GunSan (GS) AWS in the warning zone, waveform and duration were maintained, but intensity decreased significantly (figures 2(a) and (b)). Furthermore, high-frequency sea-level oscillations propagated along the coast (figures 2(c) and (d)) were coupled with air pressure oscillations. Sea-level oscillations of several centimeters, due to inverted barometer response in the open sea (Monserrat *et al* 2006), were observed with amplified wave heights of 1.0–2.5 m at most tide gauges (figures 2(c) and (d)). In contrast to the evolution of air pressure oscillations, the magnitude of sea-level oscillations gradually increased as the meteotsunami propagated toward the coast, and waveform and duration tended to vary between sites. In summary, the characteristics of the tsunami-like sea-level

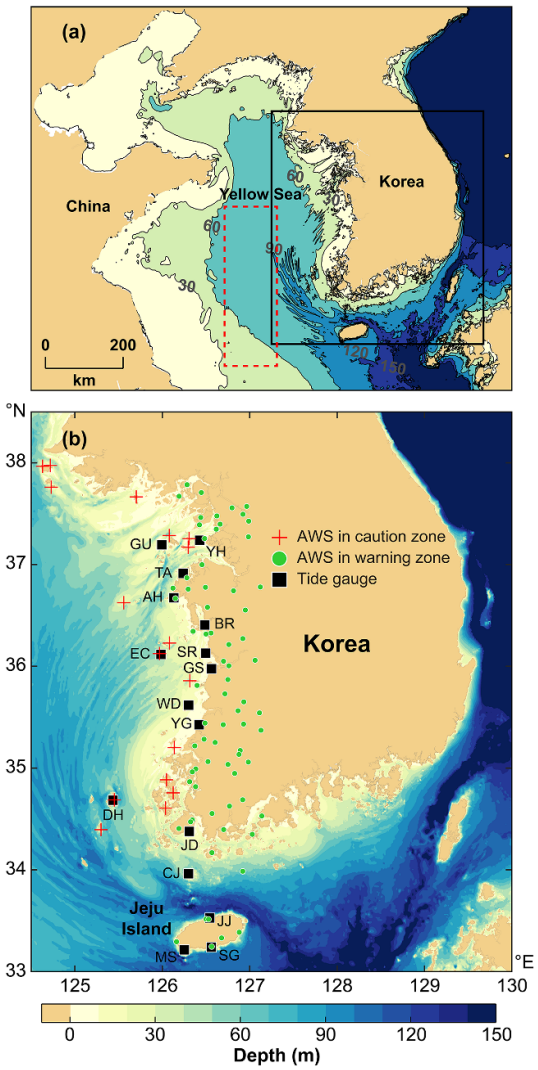


Figure 1. (a) Bathymetric map of the Yellow Sea and area where additional buoy installations are planned (red dashed box). (b) Observation systems comprising 89 automatic weather stations (AWSs): 17 AWSs in the caution zone (red crosses) and 72 AWSs in the warning zone (green circles). The following 16 tide gauges (black squares) are included in the observation systems: YeongHeungdo (YH), GulUpdo (GU), TaeAn (TA), AnHeung (AH), BoRyeong (BR), SeochunmaRyang (SR), EoChungdo (EC), GunSan (GS), WiDo (WD), YeongGwang (YG), DaeHeuksando (DH), JinDo (JD), ChuJado (CJ), JeJu (JJ), SeoGwipo (SG), and MoSeulpo (MS).

oscillations that occurred on 31 March 2007 were (a) a co-occurrence relationship with air pressure oscillations and (b) different amplification at each tide gauge.

3. Progress report on a meteotsunami monitoring system

3.1. Theoretical background

Meteotsunamis, tsunami-like waves of atmospheric origin, are characterized by the propagation resonance of forced waves locked to a traveling air pressure disturbance on the continental shelf (Monserrat *et al* 2006). When the ratio between air pressure disturbance speed (U) and long-wave phase speed (c), the Froude number ($\mathrm{Fr} = U/c$), is close to 1.0 in the open sea, coupled-mode propagation increases wave heights by continuously adding energy from air pressure oscillations moving above the ocean surface (Rabinovich 2009). During the open sea propagation stage, the atmospherically induced-forced wave (ζ_P)—the Proudman resonance—can be approximated as follows (Proudman 1929):

$$\zeta_P \approx \frac{\Delta\bar{\zeta}c^2}{c^2 - U^2} = \frac{\Delta\bar{\zeta}}{1 - \mathrm{Fr}^2} \tag{1}$$

where $\Delta\bar{\zeta} = -\Delta P_a/\rho g$ is the inverted barometer response of sea level, ΔP_a is air pressure disturbance, ρ is water density, and g is acceleration due to gravity. In the open sea, ζ_P increases as $\Delta\bar{\zeta}$ increases and Fr approaches 1, and the general resonant factor ($\zeta_P/\Delta\bar{\zeta}$) suggested by Monserrat *et al* (2006) is approximately 4–5. Although Proudman resonance conditions ($\mathrm{Fr} = 1$) are most favorable for ζ_P, free and forced ocean waves can be generated in sub-resonant ($\mathrm{Fr} < 1$) and super-resonant ($\mathrm{Fr} > 1$) environments. Amplification through the Proudman resonance is more likely to occur in a sub-resonant environment than in a super-resonant environment in various numerical simulations (Vilibić 2008).

Under Proudman resonance conditions, non-trapped long waves are amplified, propagating from the open sea to the coast. Analogously, the Greenspan resonance occurs as air pressure disturbance over a sloping shelf along the coast propagates at a speed similar to that of coastal trapped edge waves (Donn and Ewing 1956, Greenspan 1956). The speed of the edge waves (c_{edge}) trapped by topographic refraction is as follows (Ursell 1952):

$$c_{edge} = gT\tan\left[\beta\left(2n+1\right)\right]/2\pi \tag{2}$$

where β is the bottom slope, T is the edge wave period, and n is the number of zero crossings of the mode (mode number). Another external resonance between moving air pressure disturbances and open-ocean waves, shelf resonance, can be generated when air pressure disturbance and the resultant ocean waves have a period/wavelength equal to the resonant period/wavelength of the shelf area (Monserrat *et al* 2006).

In the nearshore wave transformation stage, pre-amplified and propagating meteotsunamis may be influenced by local topographical effects, such as reflection by bathymetry changes, and topographic convergence (i.e. narrowing and shoaling) in funnel-shaped bays and harbors (Vennell 2010, Pasquet and Vilibić 2013). In particular, pre-amplified long waves several centimeters high can increase to several meters when there is a resonance match between the dominant period of incoming long waves and the eigen period of the harbor, which is the harbor resonance

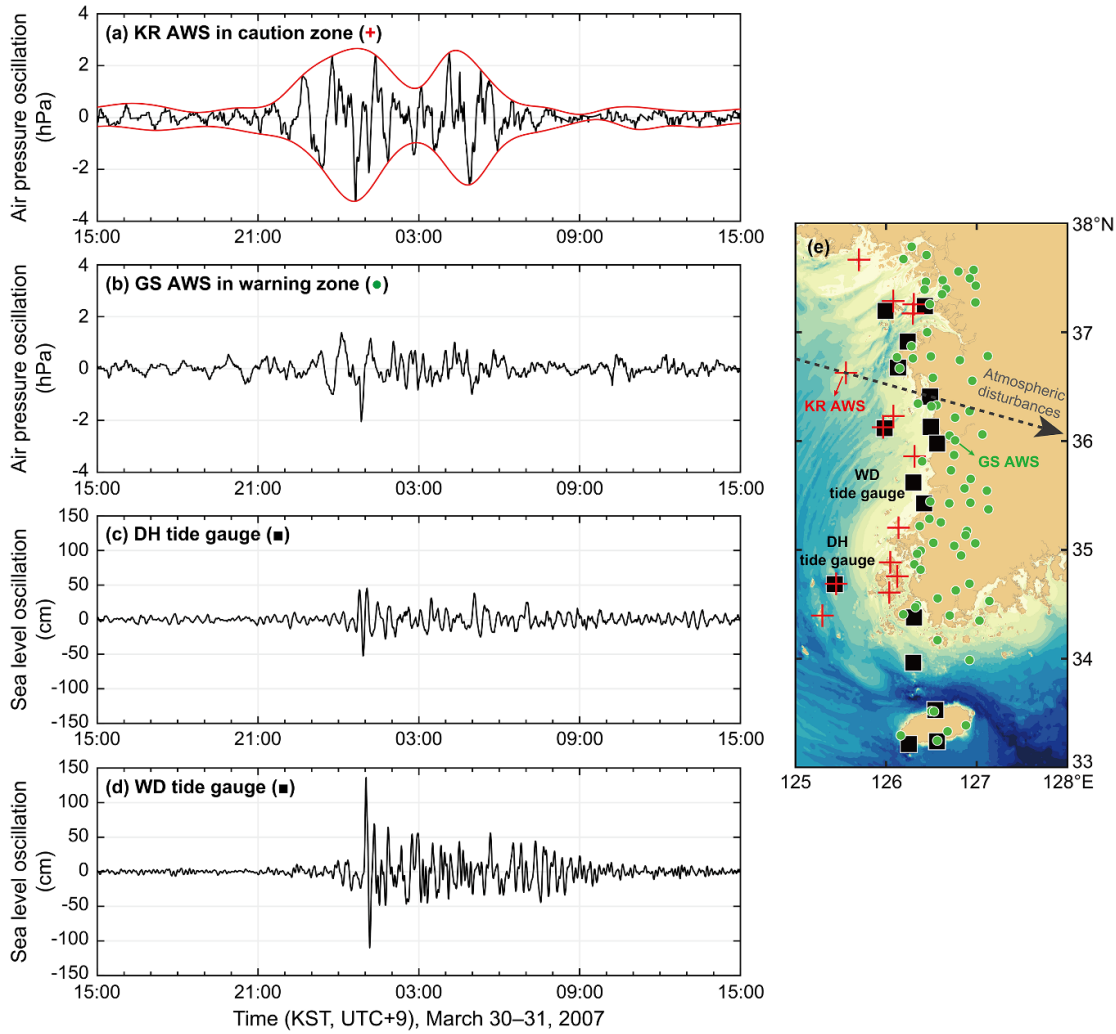


Figure 2. Characteristics of pressure-forced meteotsunamis on 30–31 March 2007. Note that the time series of air pressure and sea level were 2 h high-pass filtered using a wavelet filter (Torrence and Compo 1998). (a) Air pressure oscillation and its wave envelope at the KyukRyul (KR) AWS in the caution zone. (b) Air pressure oscillation at the GunSan (GS) AWS in the warning zone. (c) Sea-level oscillation at the DaeHeuksando (DH) tide gauge. (d) Sea-level oscillation at the WiDo (WD) tide gauge. (e) Location of AWSs and tide gauges. The propagation path of the atmospheric disturbances is indicated as a dashed arrow.

(Rabinovich 2009). The amplification factor of the internal resonance at the harbor ($H^2(f)$) can be approximated as follows:

$$H^2(f) = \frac{1}{(1 - f/f_0)^2 + Q^{-2}(f/f_0)^2} \quad (3)$$

where f is the frequency of incoming long waves, f_0 is the eigenfrequency of the harbor, and Q is the quality factor, which is an indicator of energy damping in the system (Miles and Munk 1961, Wilson 1972). Destructive meteotsunamis in harbors are the result of a double resonance effect, which is a combination of external (Proudman, Greenspan, and shelf) resonance and internal (harbor) resonance (Monserrat *et al* 2006, Rabinovich 2009). Thus, real-time monitoring of air pressure disturbance intensity and propagation in the open sea, before pre-amplified long waves enter the harbor, is crucial for effective meteotsunami warning systems.

3.2. Empirical approach to detection of air pressure oscillations

In collaboration with the KMA, we attempted to monitor tsunami-like waves and associated air pressure oscillations using the current observation system located along the eastern Yellow Sea. However, there was no observation point for an early monitoring system that could detect high-frequency sea-level oscillations directly in the open sea. Accordingly, a monitoring system was developed that could detect air pressure oscillations favorable for generating meteotsunamis based on the coupled-mode propagation of air pressure oscillation-meteotsunami (Kim *et al* 2021a). In the process of monitoring system development, empirical studies were conducted on how to

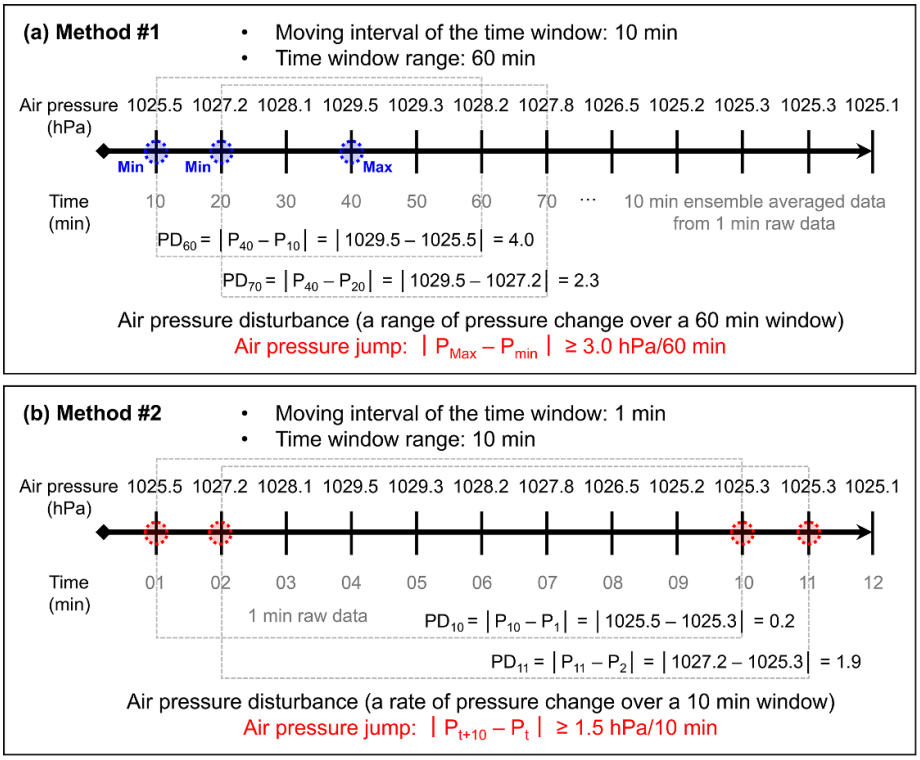


Figure 3. Methods for analyzing air pressure disturbance using (a) a range of pressure change over 60 min (method #1), and (b) a rate of pressure change (Šepić *et al* 2009, Šepić and Vilibić 2011) over a 10 min window (method #2).

assess the intensity of the air pressure oscillations (i.e. air pressure disturbance) in real time.

In our first attempt, we used a range of pressure changes (method #1) to calculate air pressure disturbances (figure 3(a)). It was assumed that significant sea-level oscillations could not be generated from a pressure change of less than 10 min. As a result, ensemble averaging was performed at 10 min intervals to denoise the raw pressure data sampled at 1 min intervals. Each air pressure disturbance was derived from a range of pressure changes over a 60 min window (i.e. range value of the six ensembles). The 60 min time window was moved at 10 min intervals in a moving average-type approach, and the air pressure disturbances were calculated using the process shown in figure 3(a). An air pressure disturbance exceeding 3.0 hPa 60 min^{-1} was considered a favorable air pressure jump for meteotsunami generation based on the minimum intensity of air pressure disturbance (method #1) during the meteotsunami events of 31 March 2007.

On 16 April 2016, the KMA encountered serious problems when testing air pressure jump detection using method #1. Although meteotsunamis were not detected at any tide gauge, two false alarms of air pressure jumps were reported at each AWS. Figure 4 shows a schematic diagram of the false alarms on 16 April 2016. A strong low-pressure system that dropped from 1008 to 988 hPa over more than 10 h was observed at most AWSs. The false alarms were reported on the descending and ascending slopes. In addition, persistent false alarms (figure 4) were reported until the maximum or minimum pressure data disappeared from the time window range of 60 min as the air pressure disturbance in the monitoring system was calculated as the range of pressure change over a 60 min window (figure 3(a)). The monitoring issues on method #1 experienced by the KMA can be summarized as follows (Kim *et al* 2021a):

(a) Air pressure jump detection using method #1 cannot capture temporal pressure changes in real time and causes persistent false alarms owing to the range value calculation method.
(b) A low-pressure system was classified as an air pressure jump because an excessively long time window range (60 min) was used.
(c) Potential meteotsunamis caused by sudden pressure changes within 10 min cannot be detected because of ensemble averaging.

To overcome the reported problems, we modified the analysis method for air pressure disturbance by using the rate of pressure change (Šepić *et al* 2009, Šepić and Vilibić 2011) over a 10 min window (method #2). Unlike method #1, it was possible to detect the real-time pressure tendency at 1 min intervals, equal to the interval of raw data, was used without denoising (figure 3(b)). In addition, the 60 min time window, which caused frequent

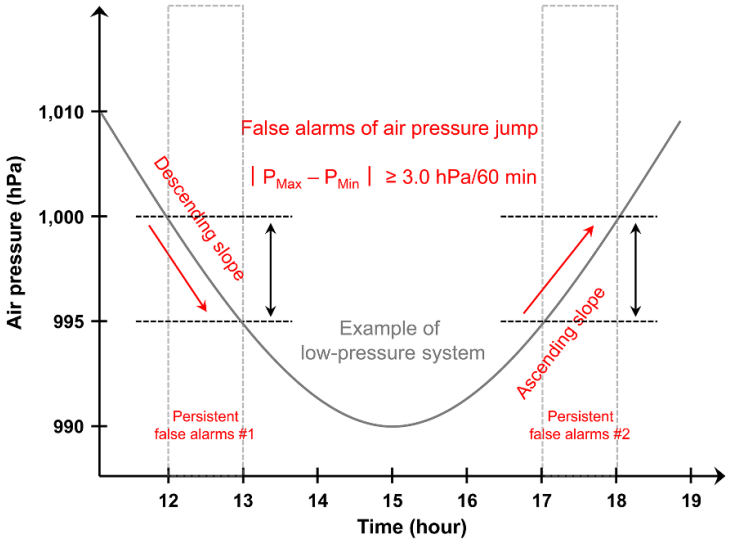


Figure 4. Example of false alarms reported during test operation of the monitoring system based on method #1 (see figure 3(a)). During a false detection on 16 April 2016, even the influence of a passing low-pressure system was considered as air pressure jumps.

false alarms during the test operation, was reduced to 10 min. As a result, the monitoring problems experienced in method #1 were addressed. The intensity threshold of air pressure jumps (1.5 hPa 10 min^{-1}) was determined based on the recommendation after a pilot test of the monitoring system from March to April 2018 (Kim *et al* 2021a).

3.3. Progress of a real-time monitoring system

Air pressure jumps that are favorable to meteotsunami occurrence in the eastern Yellow Sea can be monitored in real time using existing observation systems (89 AWSs) together with method #2. The propagation of air pressure jumps was detected using two observation systems (figure 1(b)), consisting of 17 AWSs in the caution zone (offshore islands) and 72 AWSs in the warning zone (near the coastline of the mainland). Potential meteotsunamis are considered likely to occur in the eastern Yellow Sea when the first air pressure jump is detected from at least one AWS in the caution zone, and the following air pressure jump is detected from at least one AWS in the warning zone. The propagation direction of an air pressure jump is calculated from an isochrone map, which is based on a list of air pressure jump arrival times at AWSs, and AWS position. The average speed of air pressure jumps between the two zones was estimated using the traveled distance and elapsed time from the caution zone to the warning zone along the propagation direction. The detailed protocols of the monitoring system are described in the study by Kim *et al* (2021a). Currently, the KMA operates the observation and monitoring system in real time and is responsible for sending a warning message for pressure-forced meteotsunami prevention.

In this study, we confirmed the progress of the monitoring system based on the monitoring notes from 2019. On 7 April 2019, air pressure jumps and the resultant meteotsunamis propagated intensively to the southern sea of Korea and Jeju Island (figure 5). A total of 19 AWSs and five tide gauges, where air pressure jumps-meteotsunamis were detected, are shown in figure 5(g). At 13:09 KST, the first air pressure jump was detected at the DaeHeuksando (DH) AWS in the caution zone (figure 5(a)), and the maximum intensity of the air pressure jump was detected at the KoSan (KS) AWS in the warning zone (figure 5(b)). Radar images (figures 5(e) and (f)) were used together with the monitoring system because it was not possible to estimate the spatial scale of air pressure jumps-meteotsunamis using the AWSs and tide gauges alone. Air pressure jumps were found to propagate at an average speed of 12 m s^{-1} from 12:00 to 18:00 KST based on the arrival time list at the 19 AWSs, and radar images. Interestingly, meteotsunamis preceded air pressure jumps at the JinDo (JD) and MoSeulpo (MS) tide gauges (figures 5(c) and (d)). A possible explanation may be that long-wave phase speed was at least twice as fast as air pressure jump speed, considering that the depth range along the propagation path of the air pressure jump (figure 5(g)) was approximately 90–120 m (figure 1(b)). Therefore, to secure sufficient lead time, it is necessary to install multiple meteorological stations near the western sea of Jeju Island, instead of land-based stations such as AWSs. Despite these limitations, the arrival time and propagation of meteotsunamis can be estimated using the observation and monitoring system, which tracks air pressure disturbances detected at multiple AWSs.

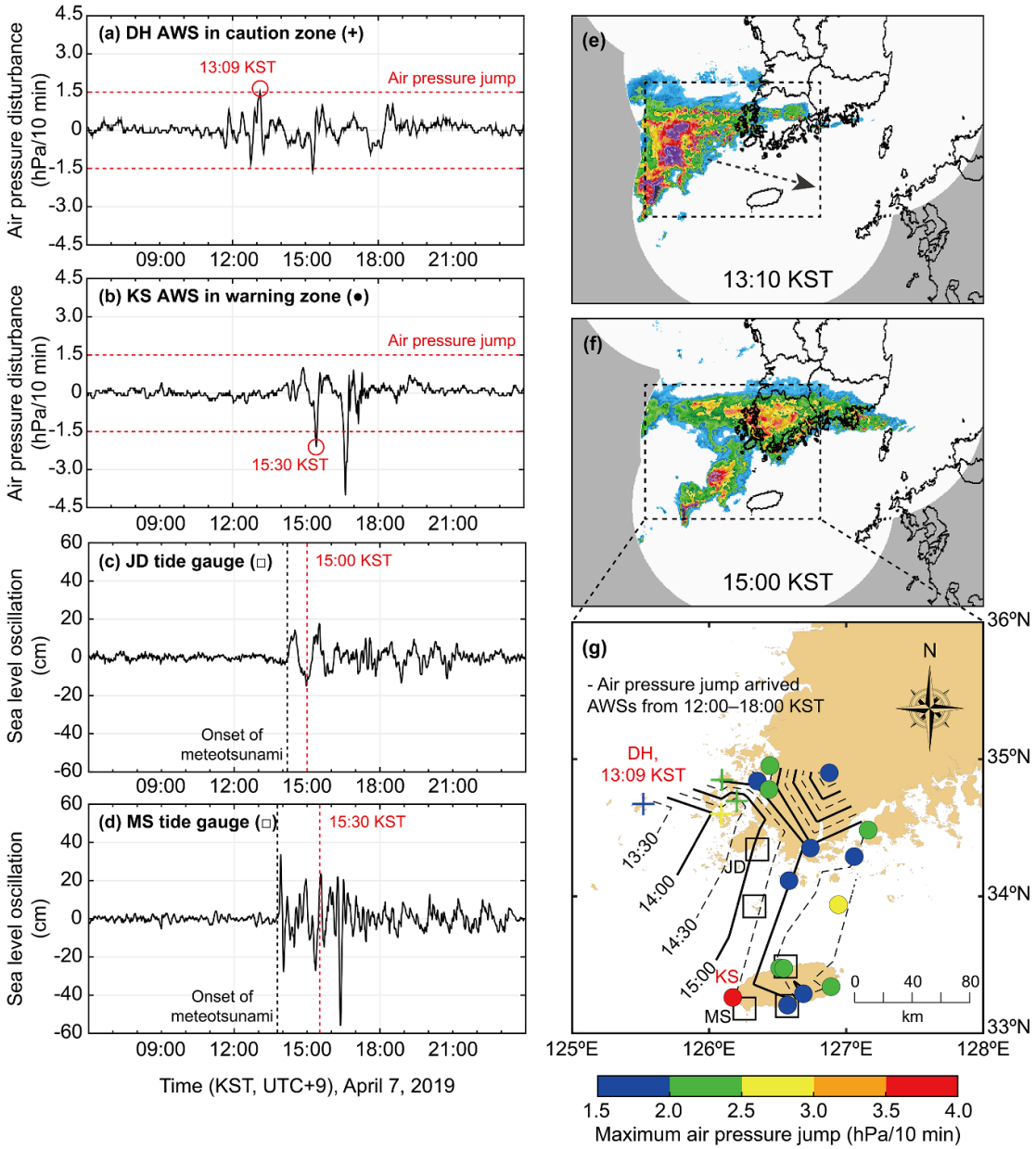


Figure 5. Progress report of the meteotsunami monitoring system: propagation of air pressure jumps using method #2 (see figure 3(b)) and resultant meteotsunamis on 7 April 2019. (a), (b) Air pressure disturbance at the DaeHeuksando (DH) and KoSan (KS) AWSs in the caution (crosses) and warning (circles) zones, respectively. (c), (d) Sea-level oscillation and arrival time of air pressure jump-meteotsunami (red and black dashed lines) at the JinDo (JD) and MoSeulpo (MS) tide gauges (black empty squares). (e), (f) Radar images at 13:10 and 15:00 KST. (g) Isochrone map of the air pressure jumps and the meteotsunamis arrived tide gauges. The first air pressure jump was recorded at the DH AWS in the caution zone. The color bar indicates the intensity of the maximum air pressure jump from 12:00 to 18:00 KST.

4. Discussion and conclusions

Our most important result is that there was insufficient lead time during real-time operation of the current monitoring and observation system. As the 17 AWSs in the caution zone are distributed extensively on the offshore islands near the coastline, lead time may be insufficient depending on the propagation pattern of air pressure jumps. In particular, when a cluster of air pressure jumps is heading to the southern Yellow Sea and Jeju Island, early warning is limited—preventing timely evacuation (figure 5). This limitation exists as there are no AWSs in the western and northern sea areas of Jeju Island (figure 1(b)). In modern tsunami science, attempts to develop reliable remote monitoring and early warning systems are concisely described as follows:

- Early tsunami warning and alert systems are based on real-time measurement of hydro-acoustic waves that travel at the speed of sound in water. These waves can be identified as acoustic signatures of surface gravity generated by pressure source properties (geometry and dynamics) using an inverse approach (Renzi and Dias 2014, Gomez and Kadri 2021);

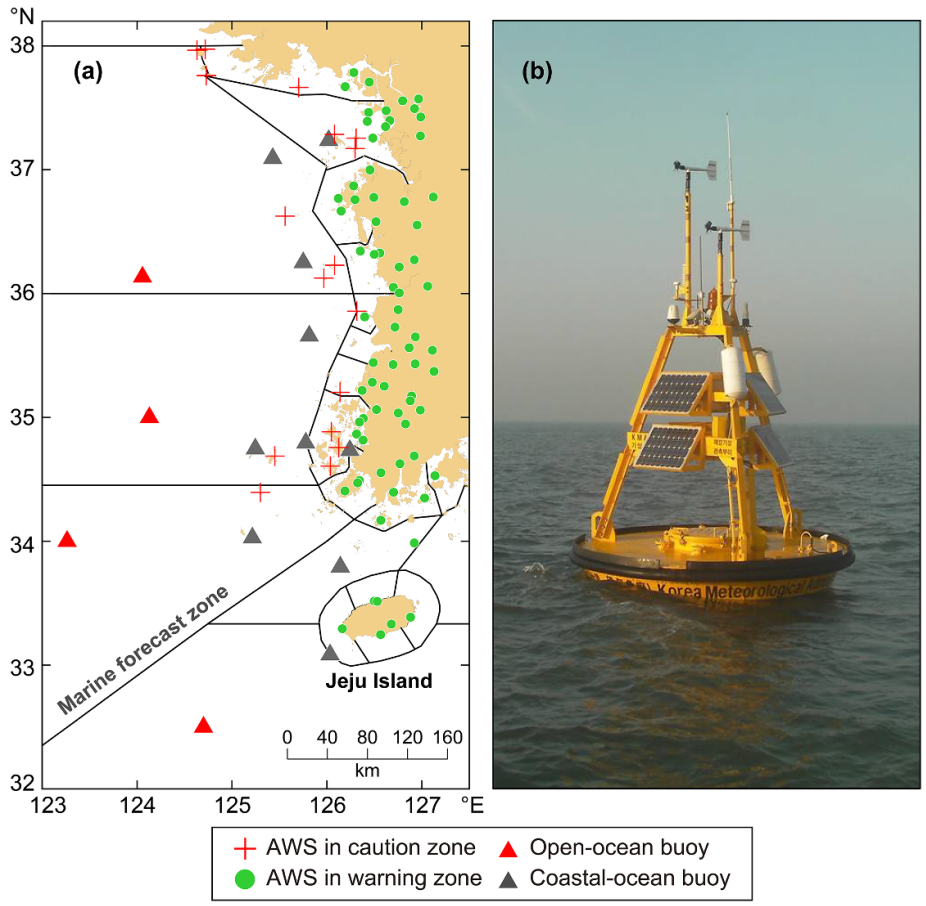


Figure 6. Current observation system and plan for observation system expansion. (a) 89 AWSs, ocean buoys with pressure sensors, and marine forecast zone. (b) Example of an open-ocean buoy installation. Reproduced with permission from the Korea Meteorological Administration (KMA).

- radar-based warning using weather radar (Wertman *et al* 2014) or high-frequency radar networks (Titov and Moore 2021); and
- meteorological and oceanographic networks from open-ocean buoys (Vilibić *et al* 2016).

To facilitate simple and low-cost early meteotsunami warnings, the KMA has initiated installation of four ocean buoys in areas beyond current radar coverage (figures 5(e) and (f)) and have been assessing their operation since 2019. The same pressure sensor with the 89 land-based AWSs will be installed in the buoys ensuring consistent monitoring of air pressure disturbances propagating from the open sea to the coast. As shown in figure 6(a), the KMA operates the segmented marine forecast zone to prepare for various natural hazards along the eastern Yellow Sea. The mooring buoys will be located in each divided area of the open sea further outside the 17 AWSs in the caution zone by 2021. The optimal sampling interval for the ocean buoys was determined to be 30 min, which takes into consideration their satellite communication and battery power limitations compared to the land-based AWSs. Therefore, it is necessary to use different methods and thresholds to define the occurrence of an air pressure jump detected by ocean buoys. Once the installation is complete, there are plans to check the sensitivity of pressure data observed in the four open-ocean buoys (figure 6(b)) and the ten coastal-ocean buoys when air pressure jumps-meteotsunamis are detected at multiple AWSs and tide gauges.

Air pressure jumps detected by the monitoring system did not always result in meteotsunamis. False-negative alarms (four air pressure jumps were detected, but only two meteotsunamis were detected) were reported during the pilot testing of the monitoring system for two months from March to April 2018 (Kim *et al* 2021a). As the intensity threshold of the air pressure jump in the eastern Yellow Sea was carefully determined based on several test operations, we assumed that the threshold was not related to false alarms. Amplification or interference near the coast could be a possible explanation for false alarms. Even if strong air pressure jumps propagate, the resultant meteotsunamis may not occur because of sudden wind gusts (Vilibić *et al* 2005, Linares *et al* 2016), tidal phases (Choi *et al* 2014), local bathymetry, and geometric features in shallow coastal waters (Ha *et al* 2014, Rabinovich 2020, Kim *et al* 2021b). These mechanisms can be accounted for by operating the atmosphere-ocean coupled model in the future.

Conversely, it is necessary to prepare for an exceptional case when air pressure jumps are not detected but meteotsunamis can occur. Under current conditions, the worst-case scenario is likely to occur when air pressure jumps propagate from south to north or locally travel to the 32–34 latitude band, including Jeju Island (figure 6(a)). There may be no warning from the monitoring system. Before the open-ocean buoys are ready for use, the potential risk of this exceptional case can be reduced by adjusting the monitoring protocol. For example, a meteotsunami warning is issued in Jeju Island when the air pressure jump propagates from a certain AWS in the caution zone to other AWSs in the caution zone, or from a certain AWS in the warning zone to other AWSs in the warning zone. It is recommended to use new methods that can be quickly adjusted in the monitoring system while maintaining the current protocol as much as possible.

Despite the limitations of lead time under specific conditions, the real-time air pressure jump monitoring system is useful and practical for meteotsunami disaster prevention in the eastern Yellow Sea. Fortunately, no damage has been reported by meteotsunamis since the development of these monitoring systems. The reported problems in the monitoring system can be addressed by (a) expanding the observation system based on marine forecast zone (figure 6), (b) adjusting the monitoring protocol, and (c) utilizing an atmosphere–ocean coupled model. Recently, we identified meteotsunami seasonality in the eastern Yellow Sea (Kim *et al* 2021b), based on historical records of pressure-forced meteotsunami occurrences over the past decade (2010–2019). More than 71% of the 42 meteotsunamis occurred during the spring to early summer (March–June) in the eastern Yellow Sea. The KMA, which monitors various disasters in real time, has trouble operating the meteotsunami monitoring system year-round because of limited labor and resources. Therefore, we plan to operate an intensive monitoring system every spring season because this is when meteotsunamis are most likely to occur.

Data availability statement

The data generated and/or analyzed during the current study are not publicly available for legal/ethical reasons but are available from the corresponding author on reasonable request.

Acknowledgments

This work was supported by Institute of Information and Communications Technology Planning and Evaluation (IITP) grant funded by The Korean Government (MSIT) (2020-0-01389, Artificial Intelligence Convergence Research Center (Inha University)). Also, this research was part of the project titled 'Improvements of ocean prediction accuracy using numerical modeling and artificial intelligence technology', funded by the Ministry of Oceans and Fisheries, Korea.

References

Choi B-J, Hwang C and Lee S-H 2014 Meteotsunami-tide interactions and high-frequency sea level oscillations in the eastern Yellow Sea *J. Geophys. Res. Oceans* **119** 6725–42

Choi B-J, Park Y and Kwon K 2008 Generation and growth of long ocean waves along the west coast of Korea in March 2007 *Ocean Polar Res.* **30** 453–66

Choi J-Y and Lee D-Y 2009 Analysis of small-scale atmospheric pressure jumps related to the generation of abnormal extreme waves at Boryeong *Ocean Polar Res.* **31** 379–88

Donn W L and Ewing M 1956 Stokes' edge waves in Lake Michigan *Science* **124** 1238–42

Eom H, Seung Y-H, Woo S-B and You S H 2012 Analysis of abnormal wave at the West Coast on 31 March 2007 *J. Korean Soc. Coast. Ocean Eng.* **24** 217–27

Gomez S and Kadri U 2021 Near real-time calculation of submarine fault properties using an inverse model of acoustic signals *Appl. Ocean Res.* **109** 102557

Greenspan H P 1956 The generation of edge waves by moving pressure distributions *J. Fluid Mech.* **1** 574–92

Ha T, Choi J-Y, Yoo J, Chun I and Shim J 2014 Transformation of small-scale meteorological tsunami due to terrain complexity on the western coast of Korea *J. Coast. Res.* **70** 284–9

Kim H, Kim M-S, Kim Y-K, You S H and Lee H-J 2017 Numerical weather prediction for mitigating the fatal loss by the meteo-tsunami incidence on the west coast of Korean peninsula *J. Coast Res.* **79** 119–23

Kim M-S, Eom H, You S H and Woo S-B 2021a Real-time pressure disturbance monitoring system in the Yellow Sea: pilot test during the period of March to April 2018 *Nat. Hazards* **106** 1703–28

Kim M-S, Woo S-B, Eom H and You S H 2021b Occurrence of pressure-forced meteotsunami events in the eastern Yellow Sea during 2010–2019 *Nat. Hazards Earth Syst. Sci.* **21** 3323–37

Linares Á, Bechle A J and Wu C H 2016 Characterization and assessment of the meteotsunami hazard in northern Lake Michigan *J. Geophys. Res. Oceans* **121** 7141–58

Miles J and Munk W 1961 Harbor paradox *J. Waterw. Harbor Div.* **87** 111–37

Monserrat S, Vilibić I and Rabinovich A B 2006 Meteotsunamis: atmospherically induced destructive ocean waves in the tsunami frequency band *Nat. Hazards Earth Syst. Sci.* **6** 1035–51

Pasquet S and Vilibić I 2013 Shelf edge reflection of atmospherically generated long ocean waves along the central US East Coast *Cont. Shelf Res.* **66** 1–8

Pattiaratchi C B and Wijeratne E M S 2015 Are meteotsunamis an underrated hazard? *Phil. Trans. R. Soc.* A **373** 1–23

Proudman J 1929 The effects on the sea of changes in atmospheric pressure *Geophys. J. Int.* **2** 197–209

Rabinovich A B 2009 Seiches and harbor oscillations *Handbook of Coastal and Ocean Engineering* (World Sci. Singapore) pp 193–236

Rabinovich A B 2020 Twenty-seven years of progress in the science of meteorological tsunamis following the 1992 Daytona Beach event *Pure Appl. Geophys.* **177** 1193–230

Renzi E and Dias F 2014 Hydro-acoustic precursors of gravity waves generated by surface pressure disturbances localised in space and time *J. Fluid Mech.* **754** 250–62

Šepić J, Denis L and Vilibić I 2009 Real-time procedure for detection of a meteotsunami within an early tsunami warning system *Phys. Chem. Earth.* **34** 1023–31

Šepić J and Vilibić I 2011 The development and implementation of a real-time meteotsunami warning network for the Adriatic Sea *Nat. Hazards Earth Syst. Sci.* **11** 83–91

Šepić J, Vilibić I and Strelec Mahović N 2012 Northern Adriatic meteorological tsunamis: observations, link to the atmosphere, and predictability *J. Geophys. Res. Oceans* **117** 4117–38

Titov V and Moore C 2021 Meteotsunami model forecast: can coastal hazard be quantified in real time? *Nat. Hazards* **106** 1545–61

Torrence C and Compo G P 1998 A practical guide to wavelet analysis *Bull. Am. Meteorol. Soc.* **79** 61–78

Ursell F 1952 Edge waves on a sloping beach *Proc. R. Soc.* A **214** 79–98

Vennell R 2010 Resonance and trapping of topographic transient ocean waves generated by a moving atmospheric disturbance *J. Fluid Mech.* **650** 427–42

Vilibić I 2008 Numerical simulations of the Proudman resonance *Cont. Shelf Res.* **28** 574–81

Vilibić I, Domijan N and Čupić S 2005 Wind versus air pressure seiche triggering in the Middle Adriatic coastal waters *J. Mar. Syst.* **57** 189–200

Vilibić I, Monserrat S, Rabinovich A and Mihanović H 2008 Numerical modelling of the destructive meteotsunami of 15 June, 2006 on the coast of the Balearic Islands *Pure Appl. Geophys.* **165** 2169–95

Vilibić I, Rabinovich A B and Anderson E J 2021 Special issue on the global perspective on meteotsunami science: editorial *Nat. Hazards* **106** 1087–104

Vilibić I, Šepić J, Rabinovich A B and Monserrat S 2016 Modern approaches in meteotsunami research and early warning *Front. Mar. Sci.* **3** 1–7

Wertman C A, Yablonsky R M, Shen Y, Merrill J, Kincaid C R and Pockalny R A 2014 Mesoscale convective system surface pressure anomalies responsible for meteotsunamis along the US East Coast on June 13th, 2013 *Sci. Rep.* **4** 7143

Wilson B W 1972 Seiches *Adv. Hydrosci.* **8** 1–94

Yoo J, Lee D-Y, Ha T, Cho Y-S and Woo S-B 2010 Characteristics of abnormal large waves measured from coastal videos *Nat. Hazards Earth Syst. Sci.* **10** 947–56

Reproduced with permission of copyright owner. Further reproduction prohibited without permission.